International Journal of Applied Earth Observations and Geoinformation 115 (2022) 103085

Contents lists available at ScienceDirect

International Journal of Applied Earth Observations and Geoinformation

journal homepage: www.elsevier.com/locate/jag

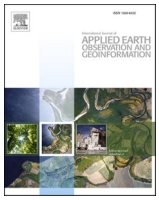

Automated mapping of glacial lakes using multisource remote sensing data and deep convolutional neural network

Saurabh Kaushik [a,b,c,*], Tejpal Singh [a,b], P.K. Joshi [d,e], Andreas J. Dietz [c]

[a] Academy of Scientific and Innovative Research (AcSIR), Ghaziabad 201002, India
[b] CSIR-Central Scientific Instruments Organisation, Chandigarh 160030, India
[c] German Remote Sensing Data Center (DFD), German Aerospace Center (DLR), Muenchener Sr. 20, 82234 Wessling, Germany
[d] School of Environmental Sciences, Jawaharlal Nehru University, New Delhi 110067, India
[e] Special Centre for Disaster Research, Jawaharlal Nehru University, New Delhi 110067, India

ARTICLE INFO

Keywords:
Convolutional Neural Network
Glacial lakes
Remote sensing
Himalaya

ABSTRACT

The characteristics of glacial lakes are a precursor to glacier retreat, ice mass loss, velocity, and potential risk of Glacial Lake Outburst Floods (GLOF). The current state of the art for glacial lake mapping, especially in a high mountainous region, is limited to manual or semi-automated threshold-based methods. Here, we propose a fully automated novel approach for glacial lake mapping using a Deep Convolutional Neural Network (DCNN) and remote sensing data originating from various sources. A combination of these multisource remote sensing data (i.e., multispectral, thermal, microwave, and a Digital Elevation Model) is fed to the fully connected DCNN. The DCNN architecture, namely GLNet, is designed by choosing an optimum number and size of convolutional layers, filters, and other hyperparameters. Our proposed GLNet is trained on 660 images covering twelve sites spread across diverse climatic and topographic regions of the Himalaya. The robustness of the model is tested over three sites in the Eastern Himalaya and one site in the Western Himalaya. The classification results outperform the existing state-of-the-art datasets by achieving 0.98 accuracy, 0.95 precision, 0.95 recall, and 0.95 F- score over the test data. The results over test sites (F-score test site1: 0.91, test site 2: 0.80, test site3: 0.97, and test site4: 0.70) showed promising results and spatiotemporal transferability of the proposed method. The coefficient of determination (R^2) between GLNet predicted lake boundaries and reference lake boundaries exhibits excellent results (0.90). The study provides proof of concept for automated glacial mapping for large geographical regions via integrated capabilities of deep convolutional neural networks and multisource remote sensing data.

1. Introduction

The global climate has shown strong warming signals in the last four decades; since 1850, every decade has been successively warmer than the preceding (Masson-Delmotte, V., P. Zhai, A. Pirani, S.L. et al., n.d.). The global surface temperature during 2001-2020 was 0.99° C higher than in 1850-1990 (Masson-Delmotte, V., P. Zhai, A. Pirani, S.L. et al., n.d.). It is unequivocal that ongoing warming exerts substantial control over the cryosphere and the resulting sea-level rise. The average global mean sea level rate increased from 1.3 mm yr^{-1} during 1901-1971 to 3.7 mm yr^{-1} during 2006-2018 (Masson-Delmotte, V., P. Zhai, A. Pirani, S.L. et al., n.d.). It is noteworthy that glacier mass and ice sheet loss played the dominant role in global mean sea level rise between 2006-2018 (Masson-Delmotte et al., n.d.). Moreover, accelerated glacier retreat (Shakun et al., 2015), ice mass loss (Hugonnet et al., 2021; Maurer et al., 2019), snow cover depletion (Mudryk et al., 2020), and permafrost thawing (Schuur et al., 2015) are excessively evident from recent studies. High Mountain Asia experiences a higher warming rate than the global mean temperature and the Northern Hemisphere. One of the obvious impacts of climate change-driven glacier retreat could be noticed as the expansion of existing lakes and the formation of new glacial lakes in the high mountainous region (Kaushik et al., 2020; Shugar et al., 2020; T. Zhang et al., 2022). These glacial lakes can be broadly subdivided into three categories 1) supraglacial lakes; these lakes are formed in a topographic depression with a gentle slope surface of a glacier, 2) proglacial lakes; lakes formed at the glacier's terminus that receive meltwater from parent glacier, 3) Others; this category is comprised of all other unconnected and high altitude glacial lakes (Chen

* Corresponding author at: Academy of Scientific and Innovative Research (AcSIR), Ghaziabad 201002, India.
E-mail addresses: saurabh21.kaushik@gmail.com, Saurabh.Kaushik@dlr.de (S. Kaushik).

https://doi.org/10.1016/j.jag.2022.103085
Received 19 July 2022; Received in revised form 20 October 2022; Accepted 27 October 2022
Available online 7 November 2022

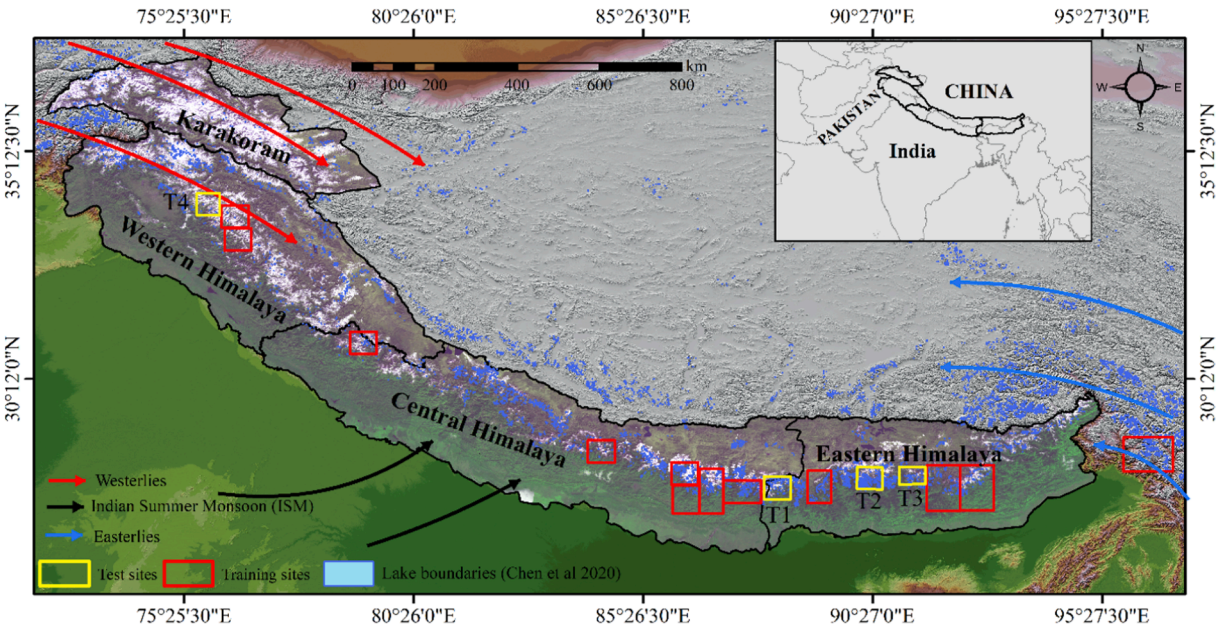

Fig. 1. Location map of chosen training (red) and test (yellow) sites across the Himalaya. The inset map exhibits the location of the Himalayan and Karakoram. The glacier lake boundaries are taken from Chen *et al.* (Chen et al., 2021). The Karakoram and Himalayan boundaries were adopted from Nie *et al.* (Nie et al., 2017).

et al., 2021). A suitable site for supraglacial lake formation is a gentle slope with low glacier velocity, the further expansion and coalescence of these supraglacial lakes may give birth to moraine-dammed lakes (Kaushik et al., 2020; Song et al., 2016). These glacial lakes play an imperative role in determining glacier response to climatic forcing, as lake-terminating glaciers are characterized by a higher mass loss and velocity (Kaushik et al., 2022a; Pronk et al., 2021). The distinct behavior of lake-terminating glaciers is mainly attributed to the buoyancy force exerted by the lake on the parent glacier, which reduces the pressure and basal resistance, resulting in a higher flow velocity (Pronk et al., 2021). Moreover, calving processes play a pivotal role in accelerated glacier melt due to the absorption of longwave radiation and lower albedo (Kaushik et al., 2022a; Pronk et al., 2021). Thereby, glacial lake presence is generally considered one of the primary contributors to the intra-regional variability in glacier velocity and ice mass loss (Dehecq et al., 2019). The presence of glacial lakes is often associated with glacier hazards, as a sudden release of water from such proglacial lakes may result into a glacial lake outburst flood (GLOF) in the downstream region (Kaushik et al., 2020; Zheng et al., 2021). A GLOF can result in catastrophic damage in the downstream region as it involves an immense volume of water and high carrying capacity of debris. Thereby, mapping and monitoring of glacial lakes have gained widespread scientific attention in the past decade owing to its feedback mechanism with parent glaciers, associated hazards, and key climate change signals.

Several researchers have exploited remote sensing capabilities for glacial lake mapping in the high mountains (Bhardwaj et al., 2015; Chen et al., 2021; Shukla et al., 2018; Wangchuk and Bolch, 2020; Wessels et al., 2002; Zhao et al., 2018) and polar regions (Dirscherl et al., 2021, 2020; How et al., 2021). Glacial lake mapping is primarily carried out using semi-automated approaches; these methods follow thresholding of Normalized Difference Water Index (NDWI) and topographic parameters (i.e., elevation and slope), as well as further manual correction of the derived results (Shukla et al., 2018). Such methods have severe limitations, as they involve human subjectivity and extensive labour, making it impractical on a regional and global scale. Moreover, the unprecedented increase in magnitude and frequency of GLOF over the last decade mandates an automated approach. In this quest, several authors propose automated approaches for glacial lake mapping using multiple thresholding or machine learning algorithms (Bhardwaj et al., 2015; Dirscherl et al., 2021, 2020; How et al., 2021; Qayyum et al., 2020; Wu et al., 2020). All of these efforts either concentrated on the polar region (Dirscherl et al., 2021, 2020; How et al., 2021) or were at a local scale (Bhardwaj et al., 2015). The method proposed by Bhardwaj et al. (2015) relies on the multiple thresholding of thermal and topographic data. The study exhibits promising results however, the applicability of the algorithm is demonstrated at a very small scale. However, the need for glacial lake mapping in high mountain regions (e.g., Himalaya and Andes) at large scale poses several specific challenges e.g., varied turbidity, shadow, wet ice, frozen lakes, seasonal snow, rock debris, vegetation presence at lower reaches, etc. (Bhardwaj et al., 2015; Kaushik et al., 2020; Wangchuk and Bolch, 2020). These challenges are accompanied by the complex topography, complicated radar backscatter, and spectral properties of land surfaces in high mountains (Wangchuk and Bolch, 2020). Thus, automated mapping of glacial lakes over large geographical regions requires a more distinct approach than the respective methods developed for polar regions. To address this key question Wangchuk et al. (2020), made a significant contribution and demonstrated a fully automated approach for glacial lake mapping across various alpine regions (e.g. High Mountain Asia (HMA), Swiss Alps, and Andes). This method incorporates multisource remote sensing data and a Random Forest Classifier; the overall accuracy of the method is reported ~97.96%. Despite the significant improvement in state-of-the-art, the proposed method contains several limitations. As it involves thresholding of radar backscatter and NDWI, the method proved to be inefficient in detecting lakes with NDWI less than 0.6 and is obscured by the layover in Synthetic Aperture Radar (SAR) back-scatter. Recently, Wu et al., (2020) exploited the Deep Learning (DL) framework (modified U-Net) for the extraction of glacial lakes in South-eastern Tibet region. The study is carried out at a local scale and does not demonstrate spatio-temporal transfer capabilities and applicability over large geographical regions. The study reported by Qayyum et al., (2020) attempted automated glacial lake mapping using VGG U-Net and efficient U-Net deep learning models. This study employed high-resolution PlanetScope imagery and still observed misclassification at lake edges primarily due to mixed ice and debris pixels or wet ice. Moreover, they essentially compare the existing model rather than any new development of a deep artificial neural network for glacial lake mapping with spatio-temporal transfer capabilities and large-scale applicability.The recent development of DeepLabv3+ model demonstrated promising results for semantic segmentation. However, classical deep learning

models, like DeepLabv3+ encounter severe limitations in satellite image segmentation (Chen et al., 2018). These limitations primarily include (1) precise delineation of ground objects; (2) spatial relationship between ground features; (3) distinguishing spectral similarity between objects (Du et al., 2021). These limitations provide ample scope to improve on the ongoing efforts of automated glacial lake mapping. To this end, the objective of the present study is to extract glacial lake boundaries relying on multisource remote sensing data and a DCNN. Here, we proposed a deep learning framework (GLNet) by adopting an optimum number and size of convolutional layers, filters, activation function, optimizer, and loss function. The present efforts are meant to develop an automated method for glacial lake mapping in highly-rugged mountain terrain with spatiotemporal transferability.

2. Materials and method

2.1. Study site

The GLNet is trained over eleven sites well distributed across the Himalaya and one site outside the Himalaya (Fig. 1). Among the twelve training sites, two are located in the western Himalaya, one is located at the trans-boundary of Western and Central Himalaya, five sites are selected from the Central Himalaya, and three sites are situated in the Eastern Himalaya (Fig. 1). The training sites are chosen to account for the variability in lake turbidity, size, geometry, and topographic parameters (e.g. elevation range, slope, and aspect) (Table S1). Glacial lakes across the Himalayan region are characterized by distinct latitudinal ranges, lake expansion rates, and precipitation sources. For example, glacial lakes in the Western Himalaya and Karakoram are characterized by smaller size, dammed by ice and dominant source of precipitation is the Westerlies (Chen et al., 2021). In contrast, Eastern Himalayan glacial lakes are larger in size, dammed by moraines, and the dominant source of precipitation is the Indian summer Monsoon (Chen et al., 2021). The test sites are purposely selected as previous studies explicitly stated that the highest GLOF risk is centered in the Eastern Himalayan region. The spatial distribution of the test sites allows us to account for all different types of glacial lakes occurring over the mountain regions.

2.2. Input data

The present study aims at exploiting the potential of remote sensing data in different electromagnetic spectrums for automated glacial lake mapping. The input layer comprises of 5 bands (B, G, R, NIR and SWIR) of Sentinel 2, Sentinel 1 (SLC, IWS) obtained coherence layer, Landsat 8 (L1TP, TIRS1), elevation layer (Advanced Land Observing Satellite (ALOS DEM); a slope layer and Sentinel-2 derived NDWI layer ((Green-NIR)/(Green+NIR)). The accuracy of glacial lake mapping is highly influenced by the scene characteristics, particularly the presence of seasonal snow, and cloud cover makes it notoriously difficult to map glacial lakes. Thereby, we consider the satellite imagery acquired during the ablation season, enabling the mapping of smaller glacial lakes. The details of data specification are displayed in Table S2. Each layer input to the GLNet represents unique characteristics that enable discrimination of glacial lake pixels from non-glacial lake pixels. For example, optical satellite imagery provides reflectance characteristics, and TIRS exhibits brightness temperature, which proved to be significant in discriminating wet ice from glacial lakes (Bhardwaj et al., 2015; Kaushik et al., 2020).

The InSAR coherence data is incorporated to exploit the loss of coherence over a glacial lake compared to the surrounding coherent surface. As several studies highlighted, lower coherence values over water bodies, particularly owing to surface smoothness which results into limited backscattering to the antenna (Lippl et al., 2018). The presence of glacial lakes is strongly associated with the elevation range therefore, the slope gradient proved to be a significant input in the semi-automated mapping of glacial lakes (Bhardwaj et al., 2015; Kaushik et al., 2020; Shukla et al., 2018). To take advantage of this fact, slope and elevation layers are fed to the GLNet. NDWI is one of the most common indicators for detecting water bodies using multispectral remote sensing data. This index utilizes the spectral reflectance of water bodies from two contrasting parts of the spectrum (i.e., maximum and minimum). The range of NDWI varies from -1 to 1, and higher NDWI values indicate a higher likelihood of the presence of a water body. Therefore, to exploit these characteristics, we feed the Sentinel-2 derived NDWI layer into the GLNet.

2.3. Methods

The proposed methodology for automated mapping of glacial lakes can be subdivided into three phases, 1) pre-processing and data preparation, 2) the designed Deep Convolutional Neural Network (DCNN), and 3) Post-processing and accuracy assessment. The pre-processing and data preparation primarily include the generation of a coherence layer, NDWI, and slope layer. Furthermore, all the layers are converted to the same spatial (i.e., 10m spatial resolution) and radiometric (16 bit) resolution. The second phase bears great significance in the proposed method, as it includes designing the DCNN with an optimum number of convolution layers, filters, and hyperparameter tuning for glacial lake mapping. In the post-processing step, background and isolated pixels are removed using ice-mask and size thresholding. To carry out all these processes, we use a combination of Sentinel Application Platform (SNAP), Quantum GIS, Arc GIS, python DL libraries (e.g., TensorFlow 2.2 and Keras 2.4), and python libraries for geospatial data (e.g., GDAL, rasterio, and pyrsgis (Tripathy, n.d.)).

2.3.1. Pre-Processing and data preparation

The pre-processing of remote sensing data and generation of training data involves the following steps.

1) Resampling: In order to maintain the consistency of the input data, we resampled Sentinel-2 SWIR band, Landsat 8 TIR, InSAR coherence images, and ALOS DEMs at 10m resolution using the nearest neighbor interpolation method in the Arc GIS 10.8 to match the spatial resolution to Sentinel-2 VNIR bands.
2) Generation of coherence layer: InSAR coherence represents the normalized complex correlation between two SAR acquisitions and indicates constant scattering within one resolution cell (Lippl et al., 2018). Mathematically it is defined as the spatial averaging of radar echoes over a coherence window (M × N pixels).

$$|\gamma| = \frac{\sum_{m=1}^{M}\sum_{n=1}^{N} S_1(m,n)S_2^*(m,n)}{\sqrt{\sum_{m=1}^{M}\sum_{n=1}^{N}|S_1(m,n)|^2\sum_{m=1}^{M}\sum_{n=1}^{N}|S_2(m,n)|^2}} \quad (1)$$

where γ = coherence coefficient of the pixel at coordinates (m, n), S_2^* = complex conjugate of S_2, M × N = coherence window, S_1 = Primary image, S_2 = Secondary image

The quality of the coherence estimation is largely influenced by thermal noise, atmospheric conditions, geometric and volume decorrelation. Theoretically, coherence values range from -1 to 1. A negative coherence value indicates minimal signal stability, whereas 1 signifies maximum coherence and stability of the signal (Lippl et al., 2018; B. Zhang et al., 2022). Here, we exploit the distinct difference between the lake characteristics from the surrounding, as glacial lakes appear darker in the SAR images due to higher specular reflectance (Zhang et al., 2019). Moreover, coherence estimation aids in the lake and wet ice and snow discrimination, as glacial wet ice moves between two SAR acquisitions. VV polarization image pairs were utilized to generate coherence images. The generation of coherence images is carried out in an automated manner using the

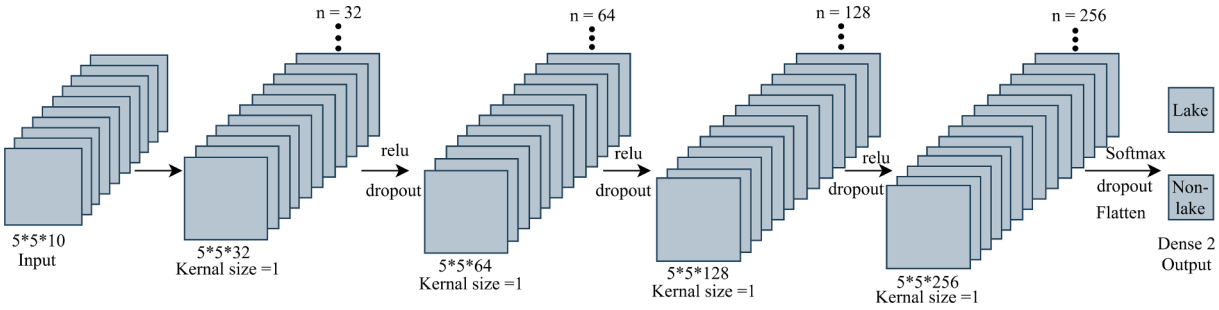

Fig. 2. Overview of the proposed GLNet. The inputs to the architecture are 10 pre-processed bands (i.e., B, G, R, NIR, SWIR, TIR, SAR coherence, slope, elevation, and NDWI). The features of the input image are an extracted series of convolution layers (encoder) and a fully connected layer (decoder) providing the final output.

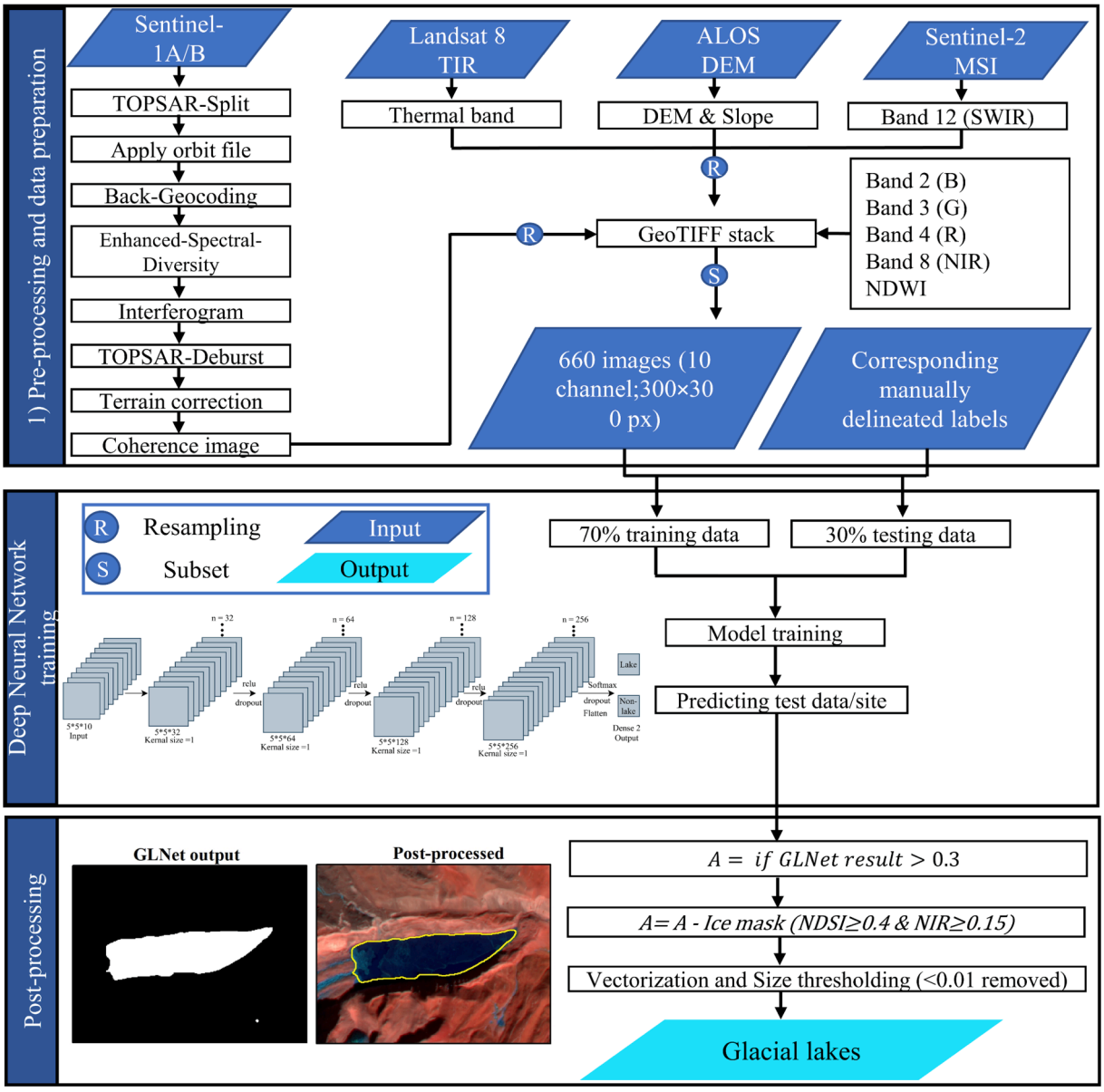

Fig. 3. The overall workflow of the proposed scheme.

SNAP graph builder (a detailed explanation is given in (Kaushik et al., 2022b; Lippl et al., 2018)).

3) Slope: To estimate the surface slope based on the ALOS DEM, we used the spatial analyst slope tool of the ArcGIS software version 10.8.2.

4) Areal extent: To keep the same extent of all the training data, images were subset to 300×300px. Finally, all layers were stacked consisting of ten bands (i.e., B, G, R, NIR, SWIR, TIR, SAR coherence, slope, elevation, and NDWI).
5) Label data generation: The available glacial lake dataset by Chen et al. (Chen et al., 2021) is used to generate the label data. The label dataset consists of glacial lakes and all possible glacial surface features (e.g. snow and ice, supraglacial debris cover, periglacial debris, flowing water and shadow) (Fig. S1 and S2). We rasterize the glacial lake polygons using the method described in (Kaushik et al., 2022b). The finally generated label data consist of glacial lake pixels labeled as 1 and the background is represented by 0. In the present study, datasets are comprised of 660 images of 300×300 extent and corresponding labels. The input data preparation did not require precise delineation of the targeted feature (i.e., glacial lakes). As DL models have shown excellent performance with a huge amount of input data with low-quality labels rather than less training data with precise-quality check labels (Xie et al., 2020; Zlateski et al., 2018).

2.3.2. Deep Convolutional Neural Network Architecture (GLNet)

The present study exploits the capabilities of a fully connected feed-forward Deep Convolutional Neural Network (GLNet) for the semantic segmentation of lake and non-lake features (Fig. 2). We designed a 2D-CNN with the architecture illustrated in Fig.2. The GLNet architecture consists of six layers, including an input layer, four convolutional layers, and a fully connected output layer. The ratio of lake and non-lake pixels is highly imbalanced in the entire dataset, as lake coverage in any scene represents a very small proportion of the entire image. To deal with this challenge, here we downsample the majority class (i.e., non-lake pixels) which resulted in significant decrease in the training sample. Further, the input data is normalized using min-max scaling prior to feeding into GLNet. The input layer has a dimension of 5×5×10, where 5×5 is the spatial dimension of the image chips with 10 channels. A smaller spatial dimension of image chips is considered to achieve higher computational efficiency. Furthermore, we increased the number of filters in the next four convolutional layers (Fig. 3) to extract the feature from the input data. To introduce the non-linearity in the model we used rectified linear unit (Relu) and Softmax activation function (Fig. 3). Mathematically, Relu is a simple function that retain the input value if its positive and returns 0 if input value is 0 or less (Eq. (2)). Eq. (3) demonstrates Relu's backpropagation function that returns backpropagation coefficient as 1 when input value is greater than 0 and returns 0 in case of input value is 0 or less. At the output layer Softmax function is applied which returns the value between 0 and 1, thus providing the probabilities for lake and non-lake pixels.

$$y = \begin{cases} x(x > 0) \\ 0(x \le 0) \end{cases} \tag{2}$$

$$\frac{dy}{dx} = \begin{cases} 1(x > 0) \\ 0(x \le 0) \end{cases} \tag{3}$$

In order to achieve the model's convergence, we used 'Adam' (Kingma and Ba, 2014) optimization algorithm. This algorithm combines the advantage of adaptive gradient and momentum computation, that can be mathematically expressed as Eq. (4). In order to deal with the bias tendency of mt and vt toward zero, bias corrected mt and vt are computed via Eq. (5). We fine-tuned the learning rate to achieve optimum gradient descent and best results are attained at 0.0001. The computation of error between predicted class and ground truth and optimal adjustment in the coefficient while performing backpropagation is carried out using sparse categorial cross entropy loss function (Eq. (6)). Furthermore, in order to avoid overfitting and achieve model's faster convergence, we used a combination of dropout (0.2) and early stop method (patience 20). This patience level indicates that the model will wait 20 epochs after insignificant improvement in the validation loss, giving a scope for additional improvement. All experiments were performed using a GeForce GTX 1080 GPU.

$$mt = \beta_1 m_{t-1} + (1-\beta_1)\left[\frac{\delta L}{\delta wt}\right] vt = \beta_2 v_{t-1} + (1-\beta_2)\left[\frac{\delta L}{\delta wt}\right]^2 \tag{4}$$

$$\widehat{mt} = \frac{m_t}{1-\beta_1^t} \widehat{vt} = \frac{v_t}{1-\beta_2^t} \tag{5}$$

$$J(w) = -\frac{1}{N}\sum_{i=1}^{N}[\widehat{y}_i \log(\widehat{y}_i) + (1-y_i)\log(1-\widehat{y}_i)] \tag{6}$$

where,

mt = aggregate of gradients at time t, δwt = derivative of weights at time t, vt = sum of square of past gradients [i.e., sum (δL /$\delta wt-1$)] (initially, $Vt = 0$), β_1 & β_2= decay rates of gradients in the momentum and RMSprop method, m_{t-1} = aggregate of gradients at time t-1, δL = derivative of loss function, $\widehat{mt}$ = bias corrected aggregate of gradients at time t, $\widehat{vt}$ = bias corrected sum of square of past gradients, (w) = weights of the neural network, y_i = ground truth, $\widehat{y}_i$ = predicted label

2.3.3. Post Processing

The proposed GLNet provides probability distribution output with glacial lakes and background pixels as a classification result. The probability distribution exhibits the probability of each pixel being a glacial lake. The automated post-processing steps were applied to finalize the GLNet derived results. To eliminate misclassified background pixels, all values lower than 0.3 are removed (Fig. 3). The lower threshold is used to reduce the probability of missing any possible lake pixels. In order to remove misclassified wet ice pixels, an ice mask ($NDSI \ge 0.4 AND NIR \ge 0.15$) is substracted from the obtained result in the previous step. In the next step, we applied vectorization of the lake boundaries. As a final post-processing step, size thresholding is used where polygons with an area size less than 0.01 km^2 are discarded from the results. Here we have not used any filtering technique to smoothen the results, as it may increase the size of many smaller lakes and introduce ambiguities in the results.

2.3.4. Accuracy Assessment

The accuracy assessment of GLNet derived lake boundaries is carried out by comparing the extracted lakes with manually generated lake boundaries delineated on the same data used for model training and testing. Here we generated our own lake boundaries instead of using any existing lake inventory. This manually delineated lake data is referred to as reference data throughout the results and discussion sections. The direct use of existing lake inventories as reference data may introduce discrencepecies, as they are generated using different sensor images, acquisition dates and scales. We calculated standard deep learning statistical metrics to assess the accuracy of GLNet derived lake boundaries. The true positive (TP), true negative (TN), false positive (FP), and false negative (FN) are determined by comparing the predicted pixel and ground truth (reference data). The accuracy is determined as:

$$\textit{Accuracy} = \frac{TP + TN}{TP + TN + FN + FP} \tag{7}$$

The precision rate, recall rate, and F1-score are standard metrics to evaluate the performance of the segmentation model for remote sensing data (Wang et al., 2020). These metrices are commonly used to evaluate the model's performance for similar tasks (Baumhoer et al., 2019; Chen et al., 2022; Dirscherl et al., 2021; Kaushik et al., 2022b). Here precision rate refers to the numbers of corcorrectly classified lake pixels out of all the classified lake pixels in the image. Whereas the recall rate shows the correctly classified lake pixels out of all the lake pixels present in the image (Lu et al., 2021). The F-score is determined via harmonic mean of precision and recall and is generally considered as a comprehensive metric to evaluate the model's performance. The evaluation of feature extraction is also assessed by area based accuracy metrics (i.e.,

Table 1
Results of the proposed GLNet on the chosen test sites.

Test sites	Accuracy	Recall	Precision	F-Score	Correctness (A_{cor})	Completeness (A_{com})	Quality (A_{qual})
Test site 1	0.99	0.94	0.87	0.91	0.83	0.94	0.79
Test site 2	0.99	0.70	0.95	0.80	0.67	0.70	0.52
Test site 3	0.99	0.94	1.00	0.97	0.94	0.94	0.89
Test site 4	0.99	1.00	0.54	0.70	0.54	1.00	0.54

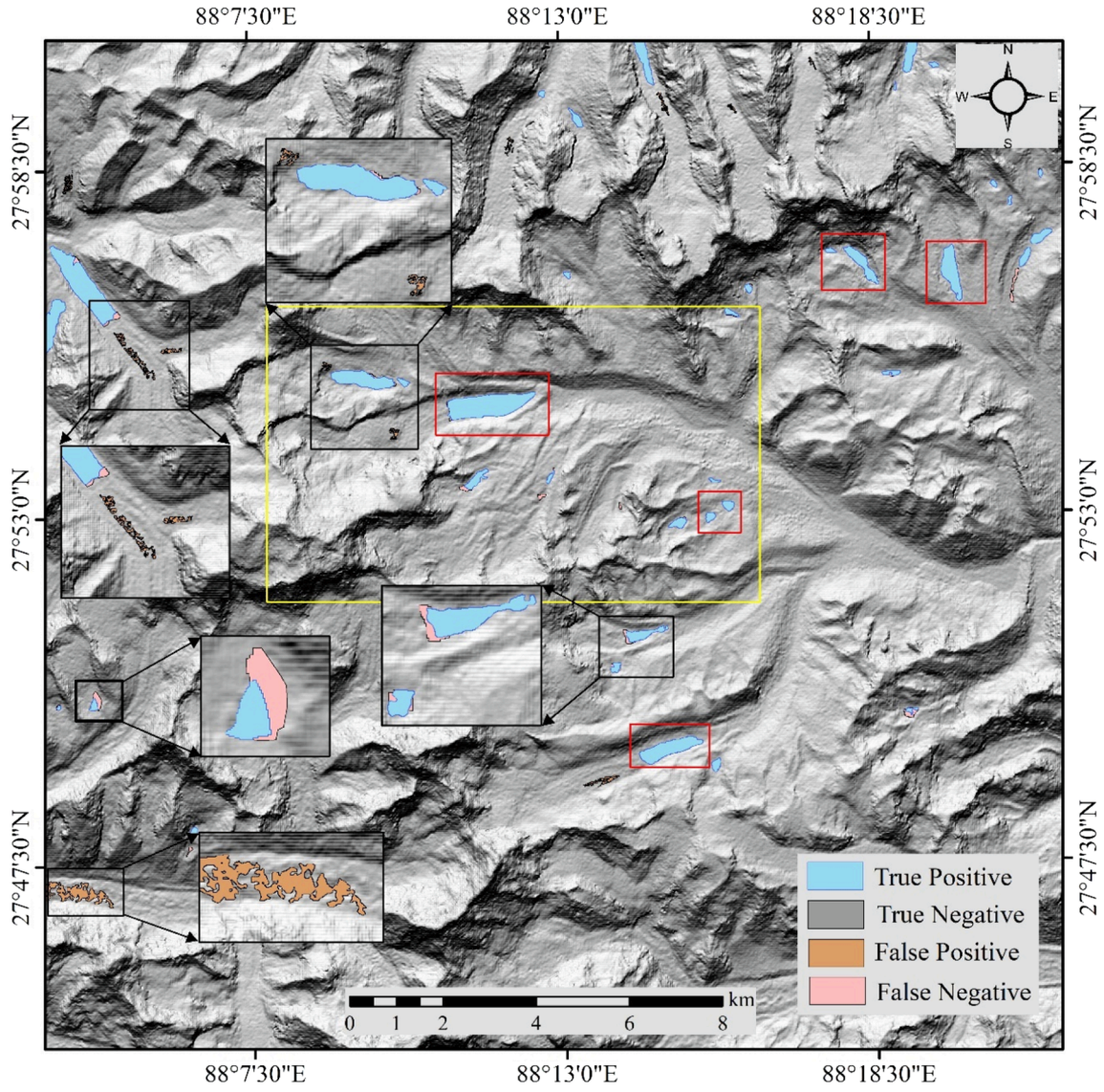

Fig. 4. Glacial lake mapping over test site 1, Eastern Himalaya using the proposed GLNet. The GLNet derived lake boundaries are compared with the reference data to estimate error of commission (FP) and omission (FN). The red and yellow rectangles show the location of lakes displayed in the Fig. 9 and Fig. 10.

completeness, correctness, and quality) (Cai et al., 2018; Tottrup et al., 2022). The correctness (A_{cor}) measure is computed as a ratio between correctly mapped area (A_C) and total mapped area (A_{Dc}) whereas, completeness (A_{com}) measure exhbits ratio between correctly mapped area (A_C) and reference area (A_{RC}). The quality metrice provides a balance between completeness and correctness (Eq. (11)). These evaluation metrics are defined as:

$$Precision = \frac{TP}{TP + FP}$$

$$Recall = \frac{TP}{TP + FN} \tag{9}$$

$$F1 - Score = 2 \times \frac{Precision \times Recall}{Precision + Recall} \tag{10}$$

$$A_{qual} = \frac{A_C}{A_{Dc} + A_{RC} - A_C} \tag{11}$$

3. Results

3.1. Proposed GLNet

The performance of the proposed DCNN (GLNet) over test data exhibits overall promising results, the model converges after 160 epochs

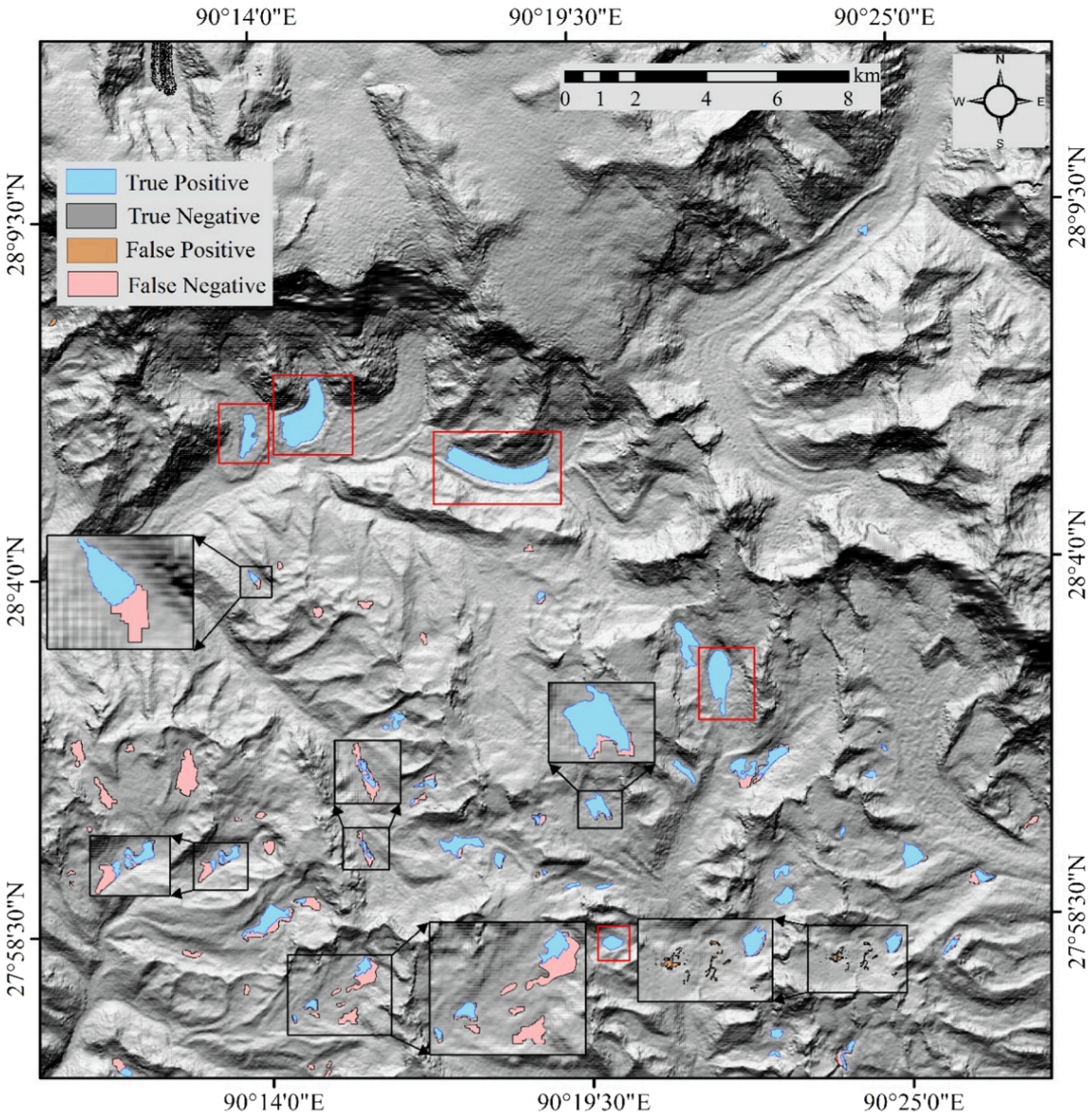

Fig. 5. Glacial lake mapping over test site 2, Eastern Himalaya using the proposed GLNet. The GLNet derived lake boundaries are compared with the reference data to estimate error of commission (FP) and omission (FN). The red rectangles show the location of lakes displayed in the Fig. 9.

(Fig. S3). The GLNet result for automated glacial lake mapping exhibits an overall 98.3% accuracy over the test areas. The other statistical metrics (precision; 0.95, recall; 0.95, F-score; 0.95) also showed promising results over the test areas. The post-processing steps significantly improved the GLNet derived results, as misclassified pixels (i.e., background and isolated) are excluded correctly. The results obtained via GLNet on three test sites were evaluated on visual comparison with reference data and estimation of the aforementioned evaluation metrics. Table 1 displays the results of GLNet on the chosen test sites. The overall results exhibit good agreement with the reference data; however, we still observe a varying degree of false positive and false negative pixels which is primarily attributed to the similar spectral, thermal, and geomorphometic (slope and elevation) characteristics of glacial lake and surrounding land features (wet ice pixels, shadows, and frozen glacial lakes). We successfully tested GLNet over a large geographical region (900 km^2; Fig. 4 and 5 and 800 km^2; Fig. 6; 1225 km^2 Fig. 7) and demonstrated its robustness in the classification of glacial lakes from surrounding land features.

3.2. Classification results for test sites (1, 2, 3 and 4)

The GLNet showed excellent results (accuracy 0.99, F1 score 0.88, correctness 0.83, completeness 0.94; Table 1) over test site 1 (900 km^2; Fig. 4). The comparison with reference data still shows few erroneous predictions (Fig. 4; Table 1). The GLNet successfully mapped 37 glacial lakes with slight areal variation (0.33 km^2). However, GLNet could not identify three small glacial lakes (0.01-0.03 km^2), which resulted in a false-negative area. We observe false-positive areas primarily in the lower zone (i.e., ablation zone) of the glaciers, as wet ice has a similar spectral response as glacial lakes. The presence of shadows in the optical data also poses severe challenges to the performance of GLNet, as shadows can be falsely predicted as lakes owing to their similar dark appearance in multispectral data. The GLNet successfully mapped 51 glacial lakes with minor areal corrections (1.77 km^2) over test site 2. We observe a comparatively low F1 score and correctness (0.80 and 0.67) over test site 2, as GLNet predicts a higher false-negative area (3.64 km^2). The false negative area mapped via GLNet is predominantly attributed to the presence of frozen or partly frozen lakes. The classification results show that GLNet missed 17 smaller glacial lakes (0.01 -

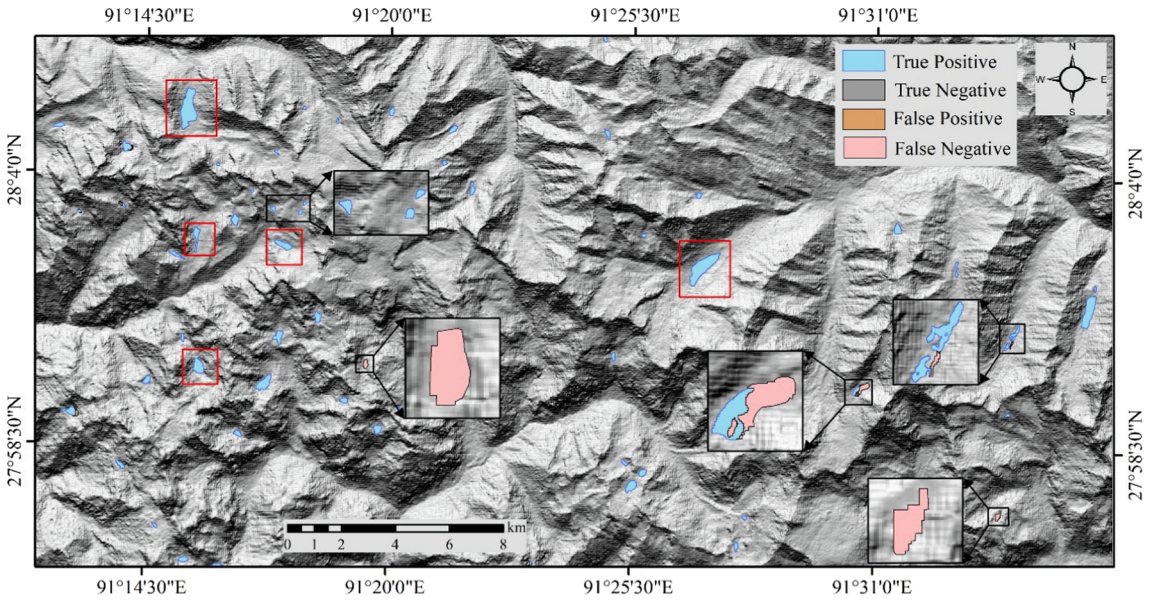

Fig. 6. Glacial lake mapping over test site 3, Eastern Himalaya using the proposed GLNet. The GLNet derived lake boundaries are compared with the reference data to estimate error of commission (false-positive) and omission (false-negative). The red rectangles show the location of lakes displayed in the Fig. 9.

0.05 km^2) over test site 2 (Fig. 5). Similar to test site 1, wet ice pixels in the glacier ablation zone and the presence of shadows in the lower valley region resulted in some false positive areas (0.44 km^2). The performance of GLNet over test site 3 (800 km^2) improved significantly, as we observed higher F1 scores of 0.97, 1.00 precision and correctness 0.94 (Fig. 6 and Table 1). The GLNet derived glacial lake boundaries matches perfectly with the reference data and exhibit only minor false-negative area (0.25 km^2). The results demonstrate that GLNet successfully mapped 58 glacial lakes over test site 3; however, it still missed two glacial lakes, which accounts for the false-negative area (0.25 km^2; Fig. 6 and Table 1). The results obtained over test site 4 exhibits promising results (accuracy; 0.99, recall; 1.00; F1 score; 0.70; completeness; 1.00; Table 1) as GLNet successfully mapped allexistingg lakes and accounts for zero false negative area (Fig. 7). However, the results show 1.07 km^2 of falsely positive mapped area primarily due to the presence of shadow.

4. Discussion

4.1. Proposed DCNN (GLNet) for glacial lake mapping

The proposed method proved to be robust in the automated mapping of glacial lakes, the comparison between GLNet derived lake boundaries and reference data exhibit excellent agreement (Fig. 4, Fig. 5, Fig. 6, Fig. 7 and Table1). The correlation analysis of GLNet derived glacial lake boundaries and reference glacial lake boundaries over all three sites exhibits good agreement (Fig. 8A). The further analysis of mapped glacial lakes demonstrates the applicability of the presented GLNet in mapping smaller glacial lakes, as 75 % of the glacial lakes detected by GLNet are <= 0.02 km^2 (Fig. 8B). These capabilities are imperative in view of several studies that highlighted the importance of small glacial lakes in terms of glacial hazards and regional climate change (Shugar et al., 2020; Zheng et al., 2021). In particular, the incorporation of multisource remote sensing data provides an edge to the presented method, as each layer has distinct characteristics which aid in distinguishing between a lake and a non-lake pixel. In order to examine the significance of each input layer in the classification of lake and non-lake pixels, we demonstrate GLNet's performance using different band combinations. In the first experiment, GLNet is trained and tested using optical data (i.e., B, G, R, NIR, and SWIR); the results showed a slight decrease in the accuracy (0.93) and F1 score (0.92) (Table 2). In comparison, when we integrated slope and elevation layers with the optical data, a slight improvement of the results (accuracy 0.95 and F1 score 0.94) could be observed (Table 2). These observations are in line with previous studies (Bhardwaj et al., 2015; Kaushik et al., 2020; Shukla et al., 2018) which highlighted the importance of geomorphologic parameters (i.e., slope and elevation) in glacial lake mapping. The results obtained via a combination of optical, slope, elevation, and NDWI (8 bands) are comparable to the GLNet trained using 10 band combination (Table 2). In contrast, the exclusion of topographic parameters (i.e., slope and elevation layers) led to a significant decrease in classification accuracy. The combination of optical, SAR coherence layer and NDWI shows an accuracy of 0.93 and an F1 score of 0.91. All these observations indicate that all 10 channels provide significant pieces of information that contribute to discriminate between the lake and non-lake pixels. Concurrently, our observations show that the combination of optical-slope-elevation-NDWI may be used to obtain the best possible results without significantly compromising the quality of results (Table 2).

4.2. Methodological advances and comparison with existing methods

The dynamic evolution of glacial lakes due to a warming climate requires a fast and reliable automated approach for glacial lake mapping. The conventional manual mapping and semi-automated approaches require extensive time and labour in the post-processing. The proposed method relied on scientific observation, gaps and recommendations identified during the last decades of research (Bhardwaj et al., 2015; Dirscherl et al., 2021; Wangchuk and Bolch, 2020; Xu, 2006). Unlike previous studies (Qayyum et al., 2020; Wu et al., 2020) here we made an attempt to develop deep convolutional neural network architecture particularly for glacial lake mapping in the Himalaya instead of using existing model architecture. In comparison to conventional manual and NDWI thresholding methods, the proposed method offers several advantages. GLNet shows promising results of automated glacial lake mapping over large geographical regions with spatiotemporal transferability. In the presented study, we successfully tested the GLNet over three test sites in the Eastern Himalaya with an area of 900 km^2 and 800 km^2 (Fig. 4, 5 and 6). In addition, one site in the Western Himalaya (1225 km^2; Fig. 7) is tested via GLNet. These four test sites represent the complexity of highly rugged terrain and all anticipated land features in mountainous terrain (e.g., glaciers, supraglacial debris, periglacial debris, river, shadow, frozen lakes, wet ice in the glacier ablation zone and vegetation presence in the lower valley region). We demonstrated

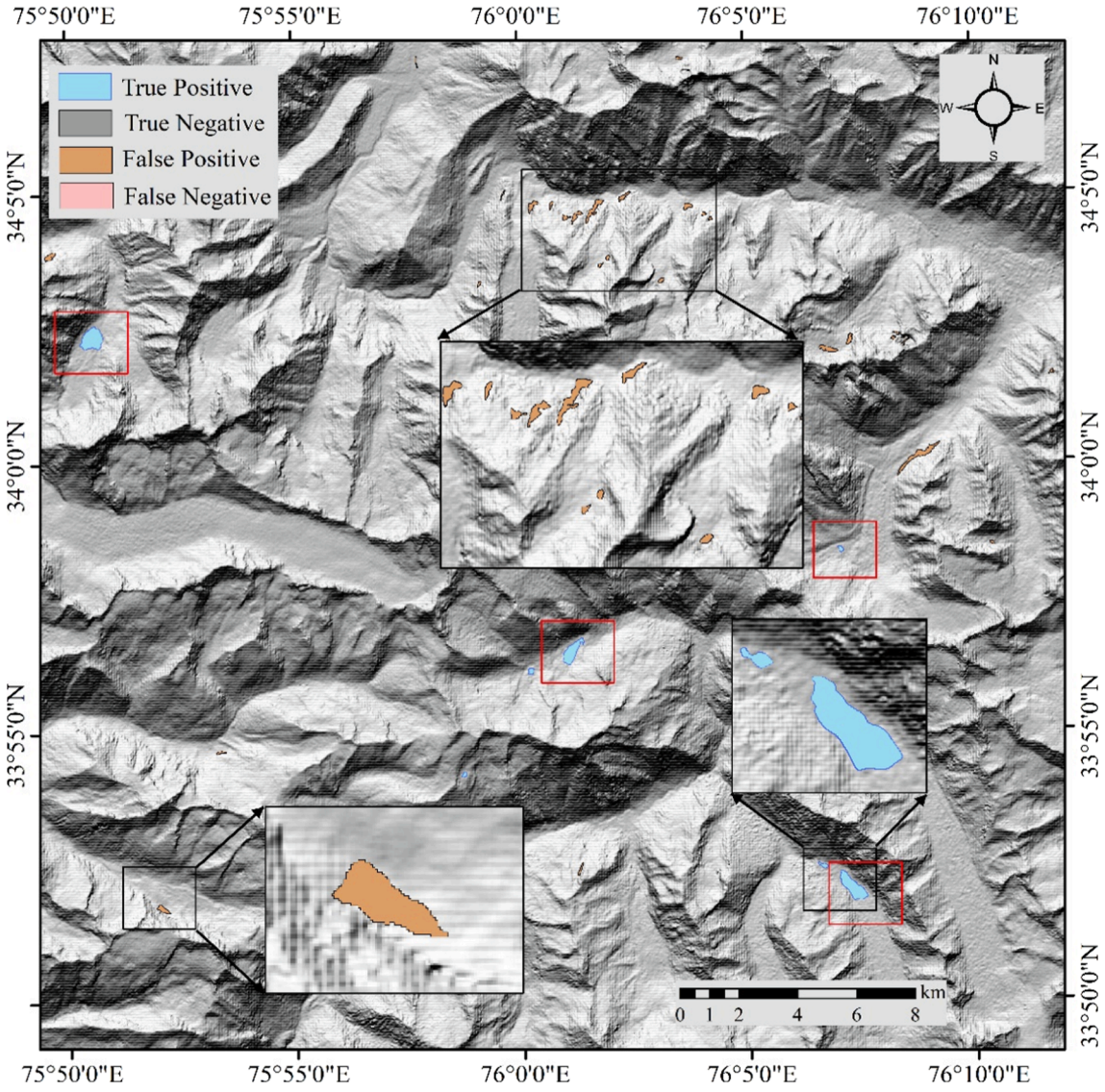

Fig. 7. Glacial lake mapping over test site 4, Eastern Himalaya using the proposed GLNet. The GLNet derived lake boundaries are compared with the reference data to estimate error of commission (false-positive) and omission (false-negative). The red rectangles show the location of lakes displayed in the Fig. 9.

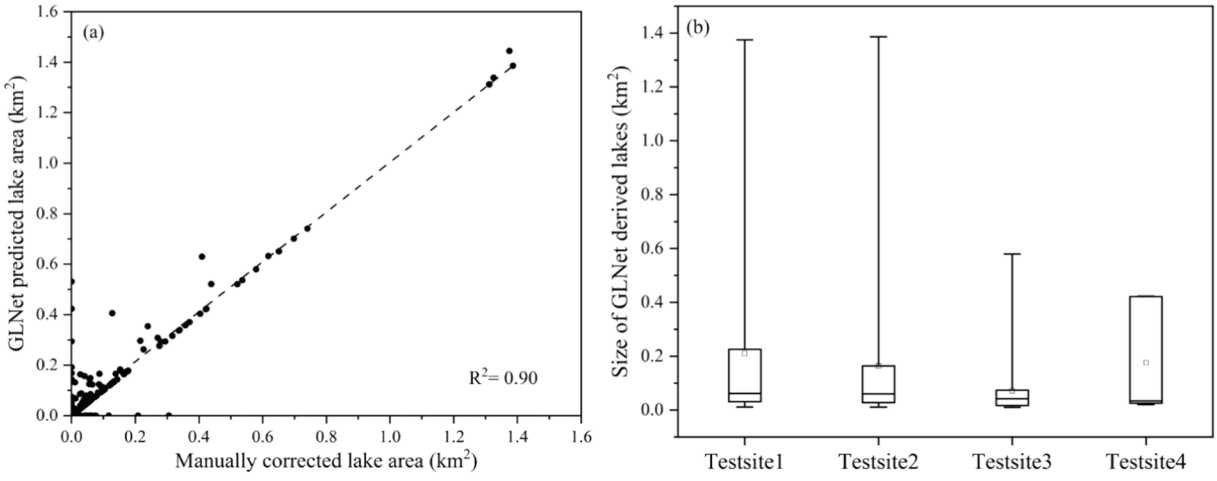

Fig. 8. The results of the proposed GLNet on all three-test site; (a) correlation analysis of GLNet derived lake boundaries and reference lake boundaries; (b) box plot showing size distribution of mapped glacial lakes via GLNet

Table 2
Results of the proposed GLNet over the test areas using different band combination. B: Blue, G: Green, R: Red, NIR: Near Infrared, NDWI: Normalized Difference Water Index

Accuracy	Recall	Precision	F-Score	Dataset Used
0.93	0.92	0.93	0.92	Optical (B-G-R-NIR)
0.95	0.94	0.95	0.94	VNIR-S-E (B-G-R-NIR-Slope-Elevation)
0.96	0.95	0.95	0.95	Optical-S-E-NDWI (B-G-R-NIR-Slope-Elevation-NDWI)
0.93	0.91	0.92	0.91	Optical-Coherence-NDWI (B-G-R-NIR-Coherence-NDWI)

the proposed method's spatiotemporal transferability, which makes it novel in the domain. However, to prove the applicability of the proposed method to other alpine regions (e.g., Tien Shan, Inner Tibet Plateau, Alpes or Andes,) or at a global scale,large-scale training data from all these regions is required to incorporate in the model. Unlike the conventional manual method (Wang et al., 2015), another key advantage this method offers is the ability to map smaller glacial lakes (0.01 km^2) (Fig. 7B). The mapping of small glacial lakes bears great significance in generating an inventory and comprehensive assessment of GLOF risks (Shugar et al., 2020; T. Zhang et al., 2022). The GLNet proved to be reliable in the automated mapping of large (> 1 km^2) and small glacial lakes (< 0.5 km^2) precisely where zero human intervention is required (Fig. 9). These lakes are the representation of varied topography, precipitation regimes, lake size, shape, appearance, and turbidity. This advantage reduces the human subjectivity involved in manually generated glacial lake inventories. We observe an exceptional performance of GLNet for glacial lakes with deep water and darker appearance (Fig. 9). Thus, the present study demonstrates the robustness of GLNet in the automated mapping of glacial lakes with spatiotemporal transferability.

Furthermore, we provide a comprehensive comparison of GLNet with commonly used NDWI thresholding and Deep Neural Network (SGDNet; (Kaushik et al., 2022b)) results particularly designed for supraglacial debris mapping (Fig. 10). The comparative analysis explicitly shows the supremacy and stability of GLNet in the precise and automated mapping of glacial lakes. The accuracy of the NDWI thresholding method is severely affected by the presence of glacial ice and thereby, the application of this method at a large scale requires extensive time in post-processing (Fig. 10B). Although, the DNN results are considerably better than the NDWI results we still observe false positive classifications of flowing water from glacier snout and glacial ice (Fig. 10C). The classification results significantly improved via the GLNet implementation, as we observed precise glacial lake mapping with fewer false positives (Fig. 10D). These observations showed that the proposed DCNN is highly capable of distinguishing river pixels and ice from glacial lakes, which remained one of the primary hinderance in the previous methods (Fig. 9). Recently, glacial lake mapping using machine (Dirscherl et al., 2020; Wangchuk and Bolch, 2020) and deep learning algorithms (Dirscherl et al., 2021) has gained wide scientific attention. Most of the automated glacial lake mapping approaches either concentrate on ice sheets or are site specific. However, Wangchuk et al. (Wangchuk and Bolch, 2020) made a significant contribution in the domain and proposed a spatiotemporally transferable method for the Alpine regions. Our proposed method offers some advantages over Wangchuk et al. (Wangchuk and Bolch, 2020). Primarily, the method proposed by Wangchuk et al. (Wangchuk and Bolch, 2020) relies heavily on the user defined thresholds of radar backscatter and NDWI maps. These thresholds are expected to vary with the spatiotemporal variability of the input data. As a result, Wangchuk et al. (Wangchuk and Bolch, 2020) explicitly highlighted the method's limitation in mapping glacial lakes entirely obscured by the layover in SAR back-scatter and lower NDWI values (0.6). In contrast, the proposed method relies on the training of a DCNN model (GLNet) which learns the intensity and spatial relationship of the input multisource remote sensing data. The threshold independent nature of the method makes it feasible to generate dynamic multi-temporal glacial lake inventories. The detailed comparison with a well-established DL based semantic segmentation model (i.e., DeepLabv3+) exhibits supremacy and stability of the proposed GLNet (Fig. 11). The results obtained via DeepLabv3+ shows numerous misclassification and imprecise delineation of glacial lake boundaries (Fig. 11), as DeepLabv3+ model is fundamentally built on the pixel-based method without incorporating the challenges of spectral heterogeneity (Du et al., 2021). The major limitation of DeepLabv3+ is that it relies on the three channels (e.g. RGB) as input, and information provided to the model proved to be inefficient for the precise delineation of glacial lakes. On the other hand, our proposed model (GLNet) successfully integrates complementary information from multisource remote sensing data and outperforms the delineation of glacial lakes with varied turbidity and indistinguishable spectral signature (Fig. 11).

4.3. Methodological limitations and future requirement

The results obtained via proposed method shows overall good agreement with the reference data; however, we still observe some erroneous prediction by the GLNet. Here, we discuss the limitation of GLNet in classifying lake and non-lake pixels and possible future work to improve the ongoing effort. The presence of shadow, wet ice in the glacier ablation zone, and frozen glacial lakes impede the performance of the proposed GLNet (Fig. 12). The presence of wet ice in the ablation zone leads to a similar spectral response as a glacial lake with low slope and high NDWI (Fig. 12A, 12B and 12D). Thus, making it indistinguishable using only optical remote sensing data. Previous studies (Bhardwaj et al., 2015; Zhang et al., 2020) explicitly highlighted the challenges posed by wet ice in automated or semi-automated mapping of glacial lakes. Thereby, to overcome this challenge we incorporated a thermal layer as one of the input layers to facilitate a distinction of lake and non-lake pixels using the brightness temperature information. Our observation shows that Landsat thermal data has limitations in distinguishing lake and wet ice pixels in several instances, primarily due to its coarse spatial resolution. However, the false-positive area (error of commission) is insignificant compared to conventional methods, which solely rely on NDWI thresholding and shadow masking. For example, including all four test sites we mapped 2.71 km^2 as a false-positive area over 3825 km^2. The detailed analysis revealed that wet ice accounts only for 0.89 km^2 (Fig. S4) out of all false positive mapped area. In addition, the presence of shadows hampers the GLNet performance primarily due to its similar dark appearance and shape (Zhang et al., 2020). Thus, it can result in false-positive areas, especially in the lower valley region (Fig.4 Fig. 5 and Fig. 7). Incorporating results from all test sites, our analysis exhibits 1.82 km^2 falsely classified shadow area as glacial lake pixels. To overcome this, we tried implementing a shadow mask in the post-processing. However, it also resulted in the loss of true positive areas (actual lake pixels). Thereby, the presence of shadow remains one of the key challenges encountered by GLNet and is susceptible to misclassification (Fig. 12C).

However, while generating glacial lake inventories these false-positive lakes could be excluded in the post-post processing step without extensive labour. Another challenge arises from the presence of frozen or partly frozen lakes. This is primarily attributed to the similar spectral and thermal response of frozen lakes and glacial ice. In this scenario, the presence of seasonal snow and smaller size makes it more indistinguishable even via manual mapping and the observation of temporal data plays a key role here. Additionally, wet ice regions also experience low slope and higher NDWI values which further makes these two classes indistinguishable at several instances (Fig. 1). To overcome all these challenges, we recommend two pragmatic strategies for future work. I) Primarily, we need to include large-scale spatiotemporal training data of wet ice, frozen lakes and shadow regions representing

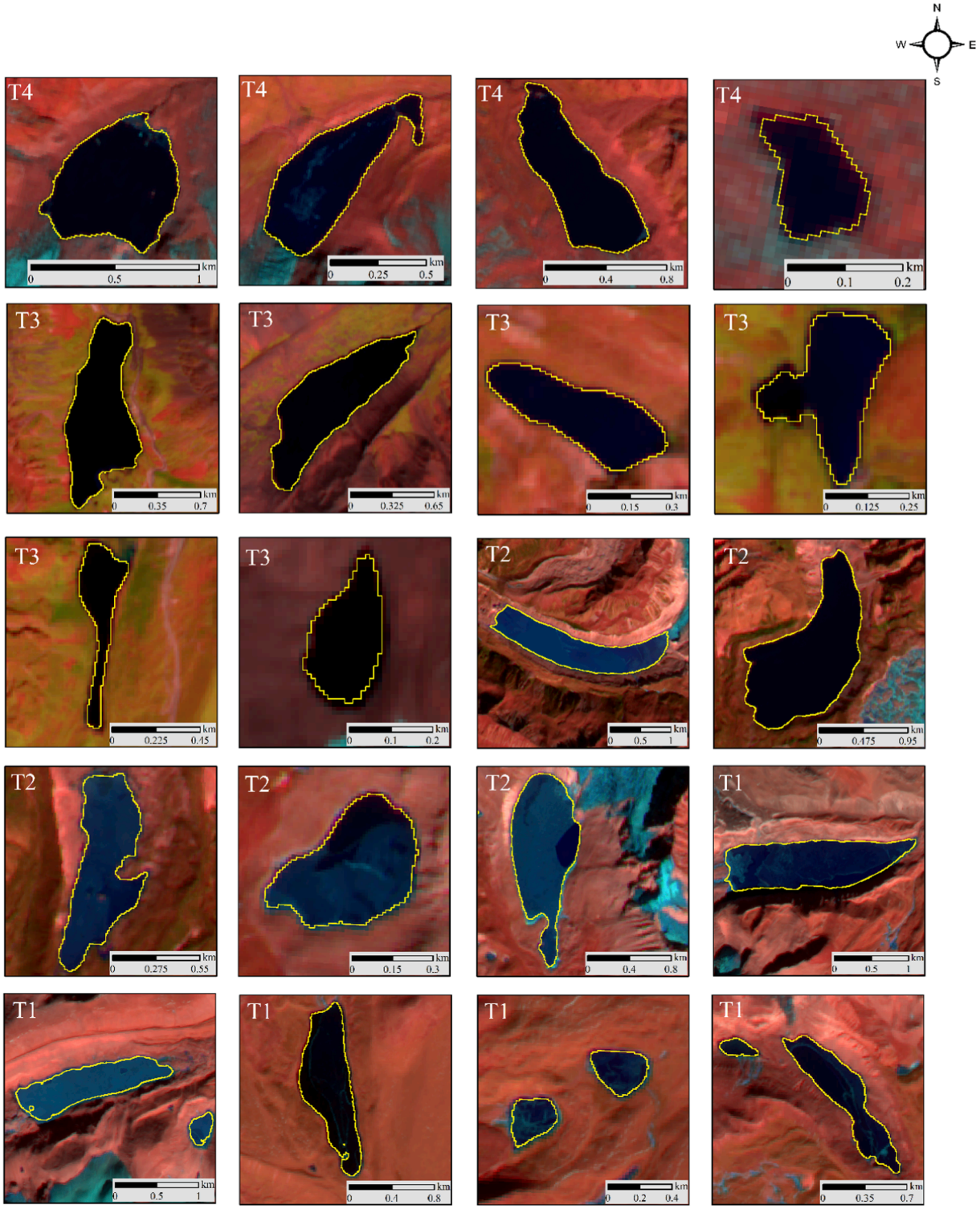

Fig. 9. Example of precise glacial lake mapping via proposed GLNet across all three test sites. GLNet successfully mapped glacial lakes of varied appearance and size across all three test sites. T1; refers to test site 1, respectively T2; test site 2, T3; test site 3 and T4; test site 4. The location of these lakes are displayed in the Fig. 4, 5, 6 and 7.

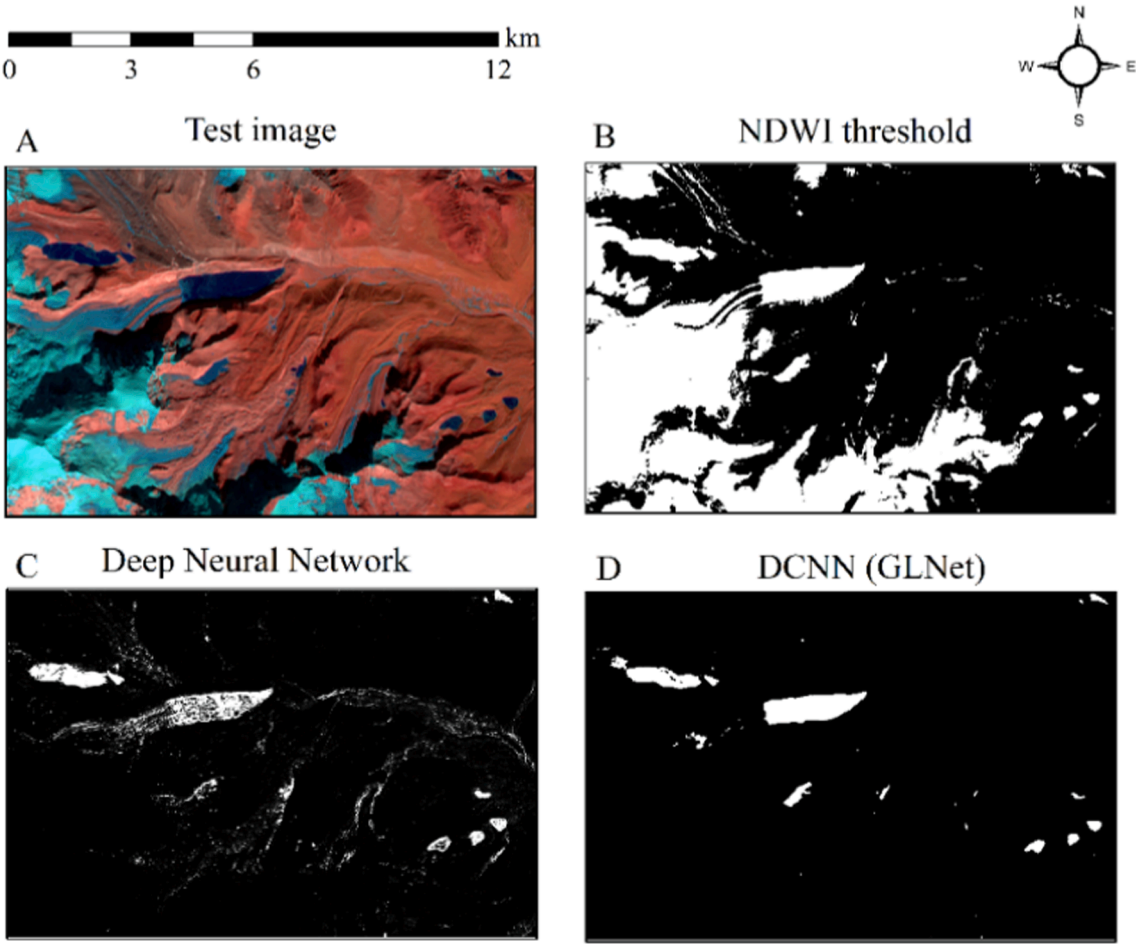

Fig. 10. Visual comparison of most commonly used method for glacial lake mapping. A) represent the test site; B) represent result derived via NDWI thresholding method; C) exhibits automated glacial lake extraction using DNN (SGDNet (Kaushik et al., 2022b)); and D) shows the results of our proposed method (GLNet) for glacial lake mapping. Contextual overview of figure is provided in the Fig. 4.

different shape, size, spectral, thermal, geomorphometric and coherence characteristics. Thus, enabling GLNet to learn more efficiently the slight difference of lake and non-lake pixels. II) Fundamentally, wet ice experiences higher velocity signals compared to lakes primarily due to ice deformation and sliding over the glacier bed under the force of gravity (Dehecq et al., 2019; Kaushik et al., 2022a). Thereby, the incorporation of a surface displacement layer using optical data or InSAR analysis may provide a useful piece of information in distinguishing two target classes. Moreover, this study provides substantial training data that could be used for developing future glacial lake mapping algorithms at a global scale, especially where GLNet fails to detect glacial lakes. The misclassified shadow pixels can also be excluded from the final results via manual correction and facilitated fast large-scale glacial lake mapping. However, here we have not performed manual correction as here study focuses on a fully automated approach. Furthermore, the incorporation of more data especially from other alpine regions of the Earth could offer a substantial opportunity to improve the deep learning model devised in the present study and help to produce consistent glacial lake datasets. The application of deep learning in glaciology is still in its infancy; we see huge potential in generating automated temporal inventories of the glacier, glacial lake, permafrost regions, and rock glaciers. Furthermore, deep learning provides a huge potential for forecasting possible future scenarios of glacier mass loss and sea-level rise.

5. Conclusion

The Himalaya is home to more than five thousand glacial lakes within complex topographic and climatic setting. The mapping and monitoring of these glacial lakes are imperative to comprehend regional climate change and mitigate the risk of GLOFs. However, automated mapping of glacial lake is primarily hindered by the presence of varying degree of turbidity, wet ice, river, vegetation at lower valley region, shadow, and frozen lakes. Here, we propose an automated approach for glacial lake mapping using DCNN and remote sensing data originating from SAR and multispectral sensors by exploiting the complementary information provided by the different electromagnetic spectra and additional products (DEM, slope, coherence and NDWI) to acquire a set of descriptors that aid better discriminating between lake and non-lake pixels. We rely on the capabilities of DCNN that simply mean that the resultant glacial lake mapping boundaries are not solely depended on the intensity variation of lake and non-lake pixels, but that additionally the spatial information between pixels also plays a pivotal role. The mapping results over the chosen test sites demonstrate the robustness of the proposed method: the model successfully classifies glacial lakes of varying size, shape, and appearance. The proposed method clearly outperformed conventional glacial lake mapping approaches relying on combined capabilities of deep convolutional network and various

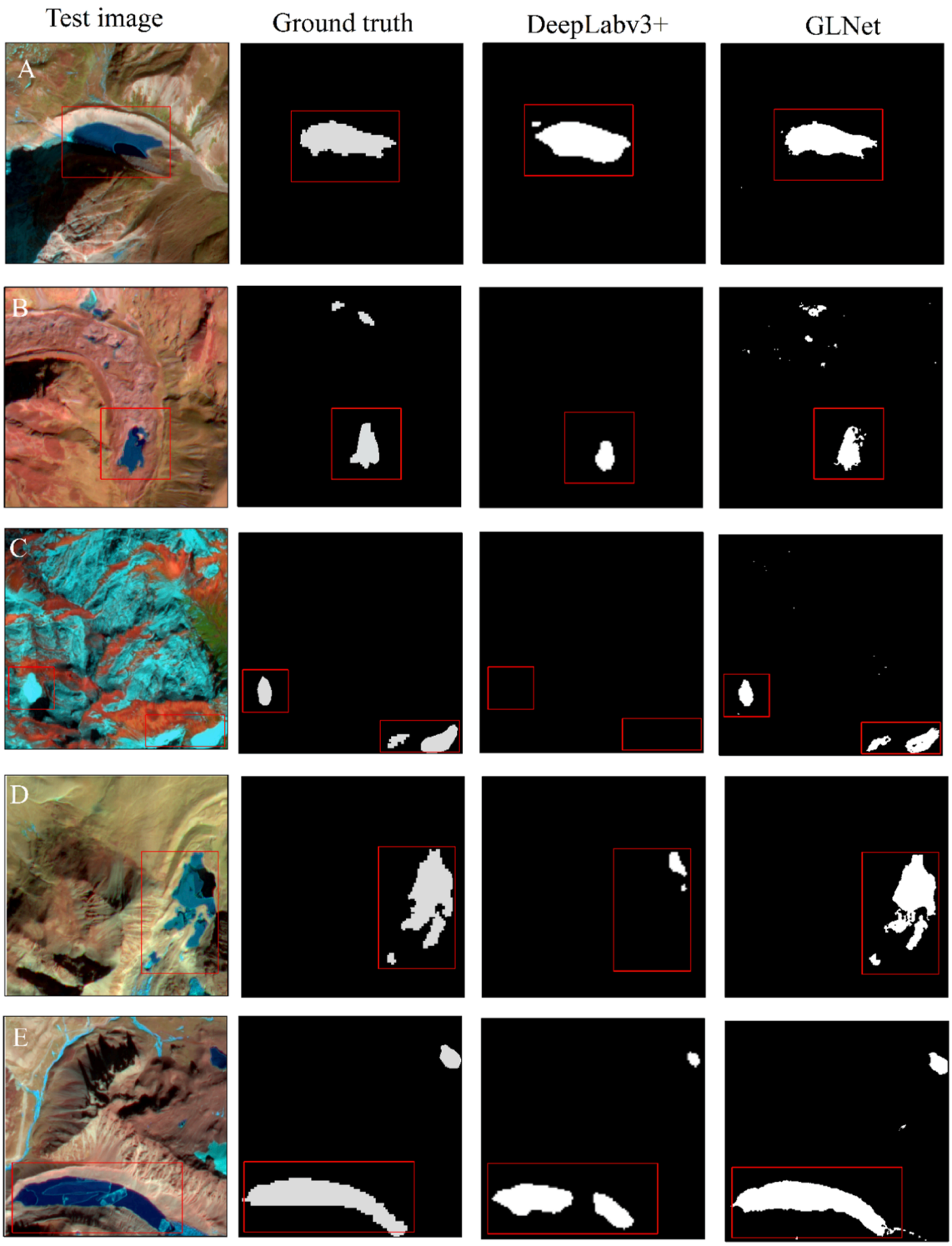

Fig. 11. Visual comparison between DeepLabV3+ and GLNet for glacial lake extraction. The GLNet outperform DeepLabV3+, as DeepLabV3+ proved to be insignificant for classifying glacial lakes with varied lake turbidity (D and E).

remote sensing data. This study makes an attempt to improve the ongoing effort of generating a consistent glacial lake dataset at high temporal and spatial resolution. In this direction, one of the key advantages this method offers is relying on open access datasets instead of commercial remote sensing data. This ensures transferability of the proposed method to other regions worldwide without limitations. The exploitation of deep learning in glaciological applications using remote sensing data provides extensive opportunities to substantially reduce labour- and time-intensive manual delineation methods and offers an automated scheme in an era where proliferation of satellite imagery has increased substantially. We strongly recommend that automated deep learning frameworks should be explored further, to establish globally applicable methods for glacial lake mapping which could provide global glacial lake datasets at unprecedented spatiotemporal scales.

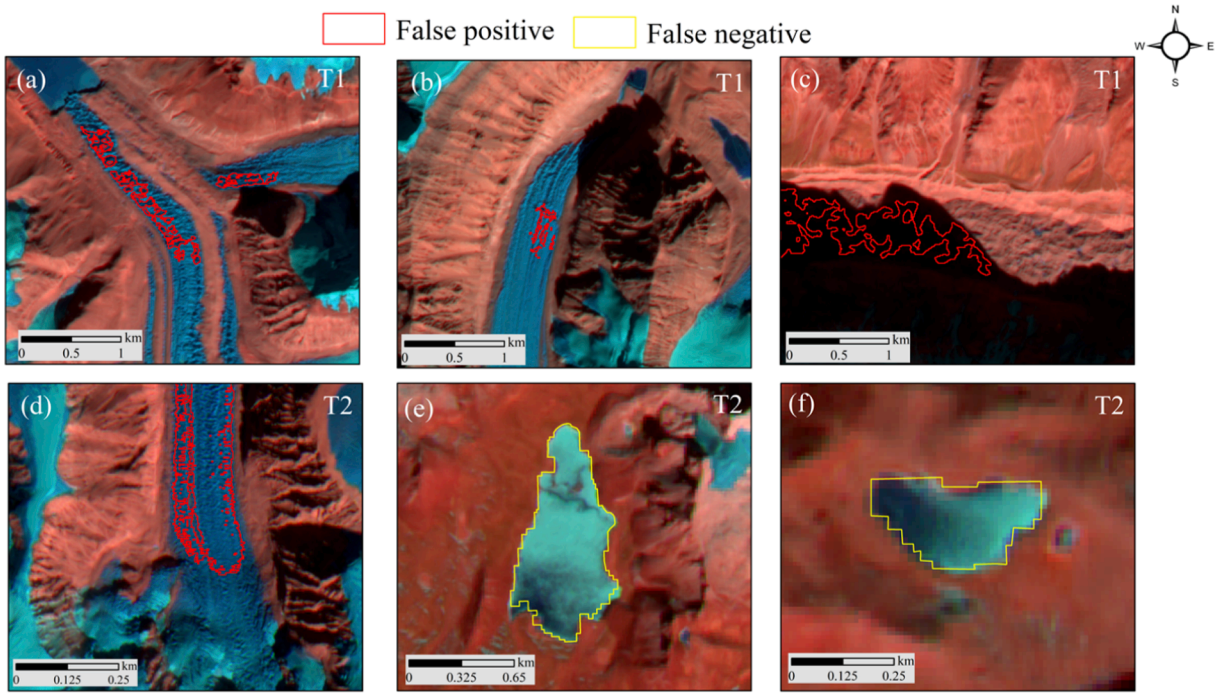

Fig. 12. Major limitation of GLNet; a, b, d represent an example of wet ice which is falsely predicted as lake over test site 1 and 2; (c) represent false prediction of shadow as a glacial lake and (e) and (f) shows false negative prediction of frozen lakes over test site 2.

CRediT authorship contribution statement

Saurabh Kaushik: Conceptualization, Data curation, Formal analysis, Methodology, Writing - original draft, Writing - review & editing. **Tejpal Singh:** Conceptualization, Supervision, Writing - review & editing. **P.K. Joshi:** Conceptualization, Supervision, Writing - review & editing. **Andreas J. Dietz:** Conceptualization, Supervision, Writing - review & editing.

Declaration of Competing Interest

The authors declare that they have no known competing financial interests or personal relationships that could have appeared to influence the work reported in this paper.

Data availability

Data will be made available on request.

Acknowledgments

SK acknowledges funding from Deutscher Akademischer Austauschdienst (DAAD) ID 2021/22 (57552338) and DST-India via INSPIRE fellowship scheme (DST/INSPIRE Fellowship/2017/IF170680). SK and TPS wish to acknowledge the Director CSIR-CSIO, Chandigarh, India, to provide the motivation for the work. PKJ acknowledges DST-PURSE of JNU, New Delhi, for providing research support. SK thanks Dr. Celia Baumhoer (DFD-DLR) and Nitin Mohan Sharma (AcSIR-CSIO), for insightful discussions on deep learning. All authors are grateful for open access satellite data distributed by ESA, USGS and JAXA.

Data availability statement

The Landsat datasets can be downloaded USGS data portal (https://earthexplorer.usgs.gov/). The ALOS Digital Elevation Models are freely available at https://asf.alaska.edu/. The Sentinel 1 and 2 data can be accessed via . The glacial lake dataset generated in the present study will be provided via DLR Geoservice.

Appendix A. Supplementary material

Supplementary data to this article can be found online at https://doi.org/10.1016/j.jag.2022.103085.

References

Baumhoer, C.A., Dietz, A.J., Kneisel, C., Kuenzer, C., 2019. Automated Extraction of Antarctic Glacier and Ice Shelf Fronts from Sentinel-1 Imagery Using Deep Learning. Remote Sens. 11, 2529. https://doi.org/10.3390/rs11212529.

Bhardwaj, A., Singh, M.K., Joshi, P.K., Snehmani, Singh, S., Sam, L., Gupta, R.D., Kumar, R., 2015. A lake detection algorithm (LDA) using Landsat 8 data: A comparative approach in glacial environment. Int. J. Appl. Earth Obs. Geoinformation 38, 150–163. 10.1016/j.jag.2015.01.004.

Cai, L., Shi, W., Miao, Z., Hao, M., 2018. Accuracy Assessment Measures for Object Extraction from Remote Sensing Images. Remote Sens. 10, 303. https://doi.org/10.3390/rs10020303.

Chen, F., Zhang, M., Guo, H., Allen, S., Kargel, J.S., Haritashya, U.K., Watson, C.S., 2021. Annual 30 m dataset for glacial lakes in High Mountain Asia from 2008 to 2017. Earth Syst. Sci. Data 13, 741–766. https://doi.org/10.5194/essd-13-741-2021.

Chen, L.-C., Zhu, Y., Papandreou, G., Schroff, F., Adam, H., 2018. Encoder-Decoder with Atrous Separable Convolution for Semantic Image Segmentation, in: Ferrari, V., Hebert, M., Sminchisescu, C., Weiss, Y. (Eds.), Computer Vision – ECCV 2018, Lecture Notes in Computer Science. Springer International Publishing, Cham, pp. 833–851. 10.1007/978-3-030-01234-2_49.

Chen, Z., Deng, L., Luo, Y., Li, Dilong, Marcato Junior, J., Nunes Gonçalves, W., Awal Md Nurunnabi, A., Li, J., Wang, C., Li, Deren, 2022. Road extraction in remote sensing data: A survey. Int. J. Appl. Earth Obs. Geoinformation 112, 102833. 10.1016/j.jag.2022.102833.

Dehecq, A., Gourmelen, N., Gardner, A.S., Brun, F., Goldberg, D., Nienow, P.W., Berthier, E., Vincent, C., Wagnon, P., Trouvé, E., 2019. Twenty-first century glacier slowdown driven by mass loss in High Mountain Asia. Nat. Geosci. 12, 22–27. https://doi.org/10.1038/s41561-018-0271-9.

Dirscherl, M., Dietz, A.J., Kneisel, C., Kuenzer, C., 2021. A Novel Method for Automated Supraglacial Lake Mapping in Antarctica Using Sentinel-1 SAR Imagery and Deep Learning. Remote Sens. 13, 197. https://doi.org/10.3390/rs13020197.

Dirscherl, M., Dietz, A.J., Kneisel, C., Kuenzer, C., 2020. Automated Mapping of Antarctic Supraglacial Lakes Using a Machine Learning Approach. Remote Sens. 12, 1203. https://doi.org/10.3390/rs12071203.

Du, S., Du, S., Liu, B., Zhang, X., 2021. Incorporating DeepLabv3+ and object-based image analysis for semantic segmentation of very high resolution remote sensing images. Int. J. Digit. Earth 14, 357–378. https://doi.org/10.1080/17538947.2020.1831087.

How, P., Messerli, A., Mätzler, E., Santoro, M., Wiesmann, A., Caduff, R., Langley, K., Bojesen, M.H., Paul, F., Kääb, A., Carrivick, J.L., 2021. Greenland-wide inventory of ice marginal lakes using a multi-method approach. Sci. Rep. 11, 4481. https://doi.org/10.1038/s41598-021-83509-1.

Hugonnet, R., McNabb, R., Berthier, E., Menounos, B., Nuth, C., Girod, L., Farinotti, D., Huss, M., Dussaillant, I., Brun, F., Kääb, A., 2021. Accelerated global glacier mass loss in the early twenty-first century. Nature 592, 726–731. https://doi.org/10.1038/s41586-021-03436-z.

Kaushik, S., Rafiq, M., Joshi, P.K., Singh, T., 2020. Examining the glacial lake dynamics in a warming climate and GLOF modelling in parts of Chandra basin, Himachal Pradesh. India. Sci. Total Environ. 714, 136455 https://doi.org/10.1016/j.scitotenv.2019.136455.

Kaushik, S., Singh, T., Bhardwaj, A., Joshi, P.K., 2022a. Long-term spatiotemporal variability in the surface velocity of Eastern Himalayan glaciers. India. Earth Surf. Process. Landf. esp.5342 https://doi.org/10.1002/esp.5342.

Kaushik, S., Singh, T., Bhardwaj, A., Joshi, P.K., Dietz, A.J., 2022b. Automated Delineation of Supraglacial Debris Cover Using Deep Learning and Multisource Remote Sensing Data. Remote Sens. 14, 1352. https://doi.org/10.3390/rs14061352.

Kingma, D.P., Ba, J., 2014. Adam: A method for stochastic optimization. ArXiv Prepr. ArXiv14126980.

Lippl, S., Vijay, S., Braun, M., 2018. Automatic delineation of debris-covered glaciers using InSAR coherence derived from X-, C- and L-band radar data: a case study of Yazgyl Glacier. J. Glaciol. 64, 811–821. https://doi.org/10.1017/jog.2018.70.

Lu, Y., Zhang, Z., Shangguan, D., Yang, J., 2021. Novel Machine Learning Method Integrating Ensemble Learning and Deep Learning for Mapping Debris-Covered Glaciers. Remote Sens. 13, 2595. https://doi.org/10.3390/rs13132595.

Masson-Delmotte, V., P. Zhai, A. Pirani, S.L., Connors, C. Péan, S. Berger, N. Caud, Y. Chen, L. Goldfarb, M.I. Gomis, M. Huang, K. Leitzell, E. Lonnoy, J.B.R. Matthews, T. K., Maycock, T. Waterfield, O. Yelekçi, R. Yu, and B. Zhou (ed, n.d. IPCC, 2021: Summary for Policymakers. In: Climate Change 2021: The Physical Science Basis. Contribution of Working Group I to the Sixth Assessment Report of the Intergovernmental Panel on Climate Chan.

Maurer, J.M., Schaefer, J.M., Rupper, S., Corley, A., 2019. Acceleration of ice loss across the Himalayas over the past 40 years. Sci. Adv. 5, eaav7266. https://doi.org/10.1126/sciadv.aav7266.

Mudryk, L., Santolaria-Otín, M., Krinner, G., Ménégoz, M., Derksen, C., Brutel-Vuilmet, C., Brady, M., Essery, R., 2020. Historical Northern Hemisphere snow cover trends and projected changes in the CMIP6 multi-model ensemble. The Cryosphere 14, 2495–2514. https://doi.org/10.5194/tc-14-2495-2020.

Nie, Y., Sheng, Y., Liu, Q., Liu, L., Liu, S., Zhang, Y., Song, C., 2017. A regional-scale assessment of Himalayan glacial lake changes using satellite observations from 1990 to 2015. Remote Sens. Environ. 189, 1–13. https://doi.org/10.1016/j.rse.2016.11.008.

Pronk, J.B., Bolch, T., King, O., Wouters, B., Benn, D.I., 2021. Contrasting surface velocities between lake- and land-terminating glaciers in the Himalayan region. The Cryosphere 15, 5577–5599. https://doi.org/10.5194/tc-15-5577-2021.

Qayyum, N., Ghuffar, S., Ahmad, H.M., Yousaf, A., Shahid, I., 2020. Glacial Lakes Mapping Using Multi Satellite PlanetScope Imagery and Deep Learning. ISPRS Int. J. Geo-Inf. 9, 560. https://doi.org/10.3390/ijgi9100560.

Schuur, E.A.G., McGuire, A.D., Schädel, C., Grosse, G., Harden, J.W., Hayes, D.J., Hugelius, G., Koven, C.D., Kuhry, P., Lawrence, D.M., Natali, S.M., Olefeldt, D., Romanovsky, V.E., Schaefer, K., Turetsky, M.R., Treat, C.C., Vonk, J.E., 2015. Climate change and the permafrost carbon feedback. Nature 520, 171–179. https://doi.org/10.1038/nature14338.

Shakun, J.D., Clark, P.U., He, F., Lifton, N.A., Liu, Z., Otto-Bliesner, B.L., 2015. Regional and global forcing of glacier retreat during the last deglaciation. Nat. Commun. 6, 8059. https://doi.org/10.1038/ncomms9059.

Shugar, D.H., Burr, A., Haritashya, U.K., Kargel, J.S., Watson, C.S., Kennedy, M.C., Bevington, A.R., Betts, R.A., Harrison, S., Strattman, K., 2020. Rapid worldwide growth of glacial lakes since 1990. Nat. Clim. Change 10, 939–945. https://doi.org/10.1038/s41558-020-0855-4.

Shukla, A., Garg, P.K., Srivastava, S., 2018. Evolution of Glacial and High-Altitude Lakes in the Sikkim, Eastern Himalaya Over the Past Four Decades (1975–2017). Front. Environ. Sci. 6, 81. https://doi.org/10.3389/fenvs.2018.00081.

Song, C., Sheng, Y., Ke, L., Nie, Y., Wang, J., 2016. Glacial lake evolution in the southeastern Tibetan Plateau and the cause of rapid expansion of proglacial lakes linked to glacial-hydrogeomorphic processes. J. Hydrol. 540, 504–514. https://doi.org/10.1016/j.jhydrol.2016.06.054.

Tottrup, C., Druce, D., Meyer, R.P., Christensen, M., Riffler, M., Dulleck, B., Rastner, P., Jupova, K., Sokoup, T., Haag, A., Cordeiro, M.C.R., Martinez, J.-M., Franke, J., Schwarz, M., Vanthof, V., Liu, S., Zhou, H., Marzi, D., Rudiyanto, R., Thompson, M., Hiestermann, J., Alemohammad, H., Masse, A., Sannier, C., Wangchuk, S., Schumann, G., Giustarini, L., Hallowes, J., Markert, K., Paganini, M., 2022. Surface Water Dynamics from Space: A Round Robin Intercomparison of Using Optical and SAR High-Resolution Satellite Observations for Regional Surface Water Detection. Remote Sens. 14, 2410. https://doi.org/10.3390/rs14102410.

Tripathy, P, n.d. pyrsgis: A Python package for remote sensing and GIS data processing.

Wang, W., Xiang, Y., Gao, Y., Lu, A., Yao, T., 2015. Rapid expansion of glacial lakes caused by climate and glacier retreat in the Central Himalayas. Hydrol. Process. 29, 859–874. https://doi.org/10.1002/hyp.10199.

Wang, Y., Lv, H., Deng, R., Zhuang, S., 2020. A Comprehensive Survey of Optical Remote Sensing Image Segmentation Methods. Can. J. Remote Sens. 46, 501–531. https://doi.org/10.1080/07038992.2020.1805729.

Wangchuk, S., Bolch, T., 2020. Mapping of glacial lakes using Sentinel-1 and Sentinel-2 data and a random forest classifier: Strengths and challenges. Sci. Remote Sens. 2, 100008 https://doi.org/10.1016/j.srs.2020.100008.

Wessels, R.L., Kargel, J.S., Kieffer, H.H., 2002. ASTER measurement of supraglacial lakes in the Mount Everest region of the Himalaya. Ann. Glaciol. 34, 399–408. https://doi.org/10.3189/172756402781817545.

Wu, R., Liu, G., Zhang, R., Wang, X., Li, Y., Zhang, B., Cai, J., Xiang, W., 2020. A Deep Learning Method for Mapping Glacial Lakes from the Combined Use of Synthetic-Aperture Radar and Optical Satellite Images. Remote Sens. 12, 4020. https://doi.org/10.3390/rs12244020.

Xie, Z., Haritashya, U.K., Asari, V.K., Young, B.W., Bishop, M.P., Kargel, J.S., 2020. GlacierNet: A Deep-Learning Approach for Debris-Covered Glacier Mapping. IEEE Access 8, 83495–83510. https://doi.org/10.1109/ACCESS.2020.2991187.

Xu, H., 2006. Modification of normalised difference water index (NDWI) to enhance open water features in remotely sensed imagery. Int. J. Remote Sens. 27, 3025–3033. https://doi.org/10.1080/01431160600589179.

Zhang, B., Liu, G., Wang, X., Fu, Y., Liu, Q., Yu, B., Zhang, R., Li, Z., 2022a. Semi-Automated Mapping of Complex-Terrain Mountain Glaciers by Integrating L-Band SAR Amplitude and Interferometric Coherence. Remote Sens. 14, 1993. https://doi.org/10.3390/rs14091993.

Zhang, M., Chen, F., Tian, B., Liang, D., 2019. Using a Phase-Congruency-Based Detector for Glacial Lake Segmentation in High-Temporal Resolution Sentinel-1A/1B Data. IEEE J. Sel. Top. Appl. Earth Obs. Remote Sens. 12, 2771–2780. https://doi.org/10.1109/JSTARS.2019.2900442.

Zhang, M., Zhao, H., Chen, F., Zeng, J., 2020. Evaluation of effective spectral features for glacial lake mapping by using Landsat-8 OLI imagery. J. Mt. Sci. 17, 2707–2723. https://doi.org/10.1007/s11629-020-6255-4.

Zhang, T., Wang, W., Gao, T., An, B., Yao, T., 2022b. An integrative method for identifying potentially dangerous glacial lakes in the Himalayas. Sci. Total Environ. 806, 150442 https://doi.org/10.1016/j.scitotenv.2021.150442.

Zhao, H., Chen, F., Zhang, M., 2018. A Systematic Extraction Approach for Mapping Glacial Lakes in High Mountain Regions of Asia. IEEE J. Sel. Top. Appl. Earth Obs. Remote Sens. 11, 2788–2799. https://doi.org/10.1109/JSTARS.2018.2846551.

Zheng, G., Allen, S.K., Bao, A., Ballesteros-Cánovas, J.A., Huss, M., Zhang, G., Li, J., Yuan, Y., Jiang, L., Yu, T., Chen, W., Stoffel, M., 2021. Increasing risk of glacial lake outburst floods from future Third Pole deglaciation. Nat. Clim. Change 11, 411–417. https://doi.org/10.1038/s41558-021-01028-3.

Zlateski, A., Jaroensri, R., Sharma, P., Durand, F., 2018. On the Importance of Label Quality for Semantic Segmentation, in: Proceedings of the IEEE Conference on Computer Vision and Pattern Recognition (CVPR). pp. 1479–1487.